Indian Journal of Engineering & Materials Sciences
Vol. 27, February 2020, pp. 96-103

Effect of alumina impurity on microstructure and properties of alumina based conventionally brazed joints

Nandadulal Dandapat & Sumana Ghosh*

Bio-ceramics and Coating Division, CSIR- Central Glass and Ceramic Research Institute, Kolkata 700 032, India

Received: 11 December 2018; Accepted: 22 August 2019

Mo-Mn metallization of alumina ceramics of different purity has been performed at 1400 °C for 10 min in moist hydrogen and nitrogen atmosphere. Nickel coating has been applied onto the metallized alumina ceramics at 1000 °C for 1 h in a reducing hydrogen atmosphere. Finally, metallized and nickel coated alumina ceramics has been brazed with another metallized and nickel coated alumina ceramics using CuAg filler alloy at 900 °C for 10 min in a vacuum furnace at 1×10^{-6} Torr pressure. X-ray diffraction (XRD), scanning electron microscopy (SEM) and energy dispersive X-ray (EDX) analysis has been carried out for phase analysis, microstructural investigation and elemental composition analysis. The adhesive strength of the metallizing layer and brazing strength of the joint have been measured by pull down breaking strength method. SEM study has shown that the width of the interfacial reaction region between the metallizing layer and substrate enhances with increasing the impurity content in the alumina ceramics. It has been observed that the adhesive strength of the metallizing layer depends on the interfacial reaction layer thickness. The adhesive strength of the metallizing layer has been increased with increasing the thickness of interfacial reaction layer. High adhesive strength of the metallizing layer as well as brazing strength has beenachieved for alumina ceramics with high impurity content.

Keywords: Alumina ceramics, Impurity effect, Metallization, Brazing, Microstructure, Characterization, Adhesion, Brazing strength

1 Introduction

The demands of the advanced ceramics like alumina, zirconia, aluminium nitride, silicon carbide are increasing day to day for very high power electrical applications like feed through, microwave tube[1-9] due to their favorable properties such as high hardness, high electrical resistivity and high melting temperature. Ceramic to ceramic joining is needed for the fabrication of high power microwave tubes (Kylstron, TWT, Magnetron etc.). As the machining of alumina ceramics is very difficult so the joining of alumina ceramics is required for the structural applications. But, the wettability of alumina ceramics is very poor. A well-known process called Mo-Mn metallization is used to increase the wettability of alumina ceramics. Wettability can be further improved by applying nickel coating onto the Mo-Mn metallized alumina ceramics. High temperature brazing is needed for microwave tube applications. The joint should be stable during actual application in a thermal cycling environment when there are gradual changes of thermal expansion coefficient (TEC) between ceramics and metal. Otherwise the joint will be cracked due to generation of thermal residual stress at the metal-ceramic interface[10,11].

The metallization of alumina ceramics has been already carried out and reported elsewhere[4,5]. Subsequently, active metal brazing has been effectively used to fabricate alumina based joints for electron tube applications[6-8]. In the present study, attempt has been made to study the effect of impurity in alumina ceramics on the microstructure and properties of the Mo-Mn metallizing layer. Further investigation has been also carried out to examine the effect of metallizing layer property on the microstructure and properties of alumina joint formed by conventional brazing method.

2 Materials and Methods

2.1 Preparation of alumina specimens and characterization

Alumina powders (92 wt.%, 96 wt.%, 99.99 wt.%) were prepared by mixing Rajmahal china clay, CaF_2 (S.D. Fine-chem Ltd.), and MgF_2 (S.D. Fine-Chem Ltd.) with alumina powder in a planetary ball mill at various ratios to get the desired percentage of alumina. 92 wt.% alumina powder was prepared by mixing 92 wt.% alumina powder with 4 wt.% Rajmahal china clay, 2.5 wt.% CaF_2 and 1.5 wt.%

*Corresponding author (E-mail: sumana@cgcri.res.in)

MgF_2. On the other hand, 96 wt.% alumina powder was prepared by mixing 96 wt.% alumina powder with 2 wt.% Rajmahal chinaclay, 1.25 wt.% CaF_2 and 0.75 wt.% MgF_2. Pure alumina (Alcoa, USA) with purity 99.99 wt.% (Alcoa, USA) was bought from Alcoa, USA. The mixed powders with different compositions were iso-statically pressed at 150 MPa pressure in a cold isostatic pressing machine using neoprene rubber mold. The pressed samples were dried in an electrical dryer for 24 h at 100°C and then calcined at 1000 °C for 1 h. The calcined samples were machined to form cylindrical shaped samples with 12 mm diameter and 2.5 mm length. The machined samples were sintered at 1650°C for 2 h in an electrical furnace (Bysakh & Co., Kolkata). The surface of sintered sample was ground with diamond coated wheel in a grinding machine and thoroughly polished in a polishing machine (Buehler, USA) using diamond polishing paste (MetaDi, Buhler) and cloth. The polished samples were thoroughly cleaned with distilled water and acetone in an ultrasonic vibrator machine. Thereafter, the alumina samples were etched with commercial HF and HNO_3 solutions in the ratio of 1:1 for 15 min. The etched samples were properly cleaned with soap, distilled water and dried at 100 °C for 2 h. The alumina sintered specimens of different purity were thoroughly characterized in terms of apparent density, apparent porosity, water absorption, microhardness, compressive strength, flexural strength, coefficient of thermal expansion, thermal conductivity and dielectric constant. Five numbers of similar alumina samples were evaluated for each property.

2.2 Metallization and conventional brazing

Molybdenum (Mo)–manganese (Mn) paste was prepared by adding 25 wt.% organic vehicle with mixture of Mo (Merck Limited, Mumbai, India) and Mn (S. D. Fine–Chem Ltd.) powder mixed in the ratio of 80:20 and homogenized for 10 h. The Mo-Mn metal paste was screen printed on the dried alumina sample. Then, the samples were dried at 100°C for 2 h and finally metallized at 1400 °C for 10 min in a tube furnace (Nisabjee Engg. Co. (P) Limited, Kolkata, India) in an atmosphere of 75% N_2+25% moist H_2 at dew point of 20 °C. Using the same technique NiO paste was prepared and screen printed onto the metallizing layer and fired at 1000 °C for 1 h in a tube furnace under a reducing hydrogen atmosphere. Finally, two metallized and Ni coated alumina samples were thoroughly polished and cleaned. Then, the samples were sandwiched with Cu-Ag filler alloy (Rupatam 35) and placed in a vacuum furnace (Hindhivac Private Limited, Bangalore, India). Thereafter, the sample assembly was brazed at 900 °C for 10 min in a vacuum of 1×10^{-6} Torr.

2.3 Evaluation of brazed joints

Phase analysis of the specimen was carried out by X-ray diffraction (XRD; PW 1710, Philips Research Laboratory, Eindhoven, The Netherlands) using CuKα radiation (45 kV, 35 mA). Microstructural observations were performed by scanning electron microscopy (SEM; Phenom Pro-X, The Netherlands) and elemental composition was determined by energy dispersive X-ray (EDX) analysis (Phenom Pro-X). The adhesive strength of metallizing layer and brazing strength of the joint were measured by using a universal tester (Romulus, QUAD Group Inc., USA). Helium leak test was conducted by using a helium leak detector (Adixen, ASM 142, France).

3 Results and Discussion

Figure 1 represents the XRD analysis for the 92 wt. %, 96 wt. % and 99.99 wt.% alumina sintered ceramics. XRD analysis showed the presence of calcium aluminate, calcium alumino-silicate, α-alumina crystalline phases in the 92 wt.% and 96 wt.% alumina samples.On the contrary, α-alumina crystalline phase was only detected in the 99.99 wt.% alumina samples. The XRD data matched with the phase diagram of SiO_2, Al_2O_3 and CaO.The microstructures of alumina sintered ceramics with 92 wt. %, 96 wt. % and 99.99 wt.% alumina content are shown in Fig. 2. Globular grains were found to be present in 96 wt. % and 92 wt.% alumina content samples whereas grains with sharp edges were noted in the microstructure of 99.99 wt.% alumina ceramics. The morphology of the grain is affected by the formation of intergranularphases during sintering[12]. The presence of intergranular glassy phase resulted in globular shaped grains in case of 96 wt.% and 92 wt.% alumina sintered ceramics whereas sharp edges for 99.99 wt.% alumina sintered ceramics were noticed due to absence of the intergranular glassy phase. The area EDX showed that 94 wt. % and 96 wt.% alumina samples were composed of Al, Ca, O, Si and Mg elements (Figs 2d and e). However, only Al and O elements were present in 99.99 wt.% alumina sample (Fig. 2f). The average grain size of alumina ceramics increased with increasing the alumina content and the porosity decreased with

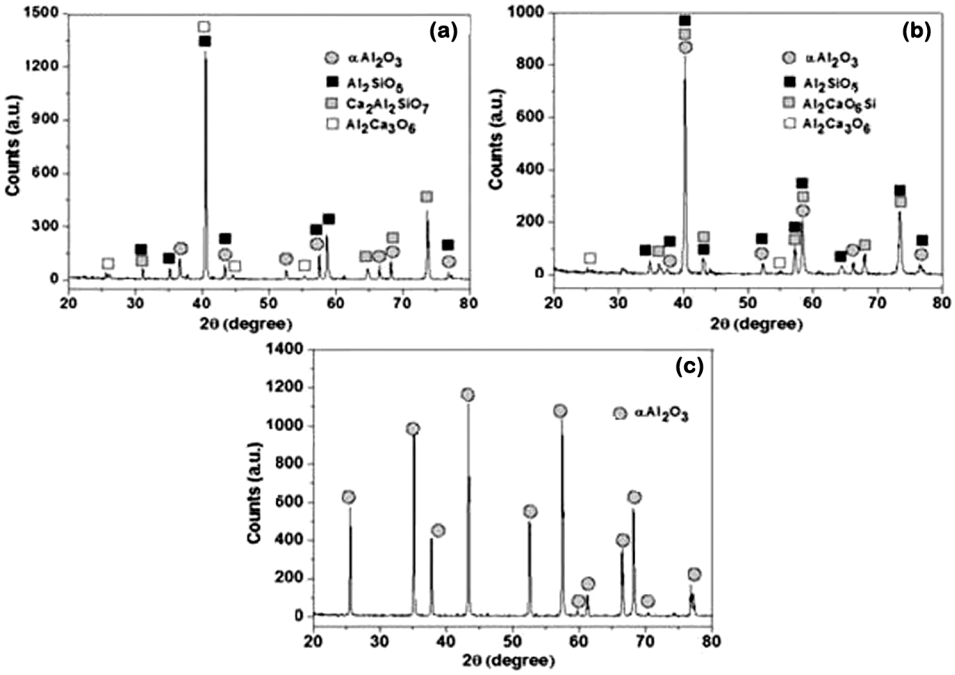

Fig. 1 — XRD patterns of (a) 92 wt. %, (b) 96 wt.% and (c) 99.9 wt.% alumina ceramics.

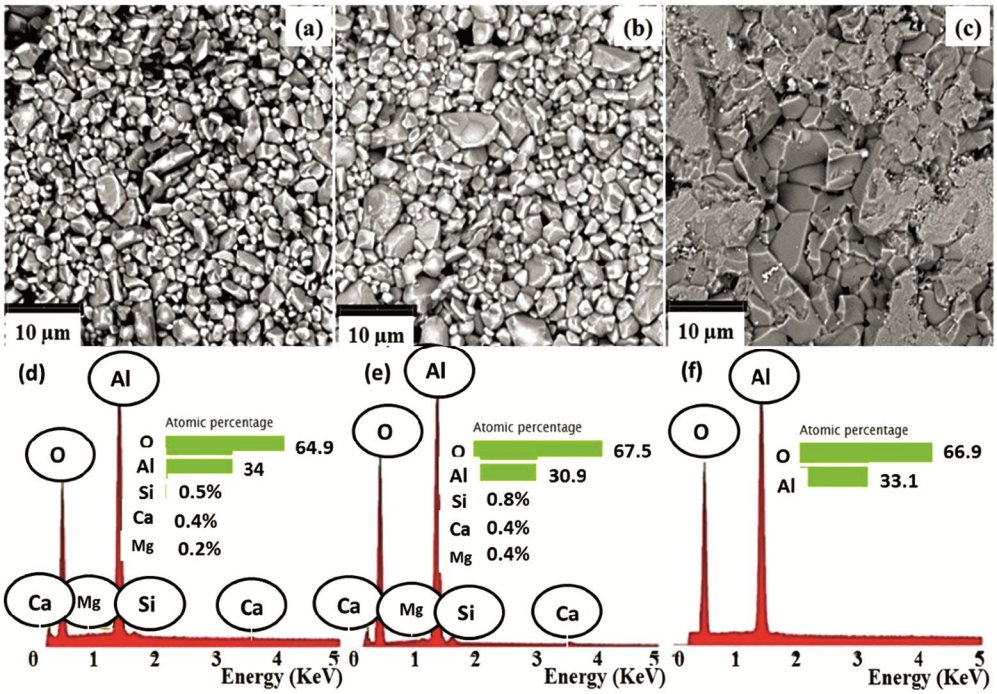

Fig. 2 — SEM images of (a) 92 wt.%, (b) 96 wt.% and (c) 99.9 wt.% alumina ceramics and corresponding EDX analyses.

increasing the alumina content. At the sintering temperature, the glass forming ingredients such as SiO_2, MgF_2, CaF_2 melted and situated at the grain boundary of alumina grains. The glassy phases at the grain boundary region increased and alumina grain size decreased with the addition of higher amount of impurity. After thermal etching at 1350 °C, glassy phases were etched out. The sintering temperature was also decreased due to the addition of impurity. Similar observation was noted by Pal *et al.*[13]. They established that the grain boundary thickness increases and alumina grain size decreases

with increasing the CaO addition from 1 wt.% to 3 wt.%.

Table 1 shows the properties of alumina ceramics with different impurity content. It was observed that the apparent density, microhardness, compressive strength, flexural strength, thermal conductivity and dielectric constant increased with increasing the percentage of alumina content. The enhancement of density with the decreaseof impurity in alumina ceramics led to improvement in the mechanical propertiesas was evident in other case also[14]. Moreover, increase in density with increasing alumina purity resulted in higher thermal conductivity and coefficient of thermal expansion[15] and dielectric constant[16]. Our previous study[4] revealed that the adhesion strength of the metallizing layer increased at higher metallization temperature. The effect of metallization temperature with respect to the adhesive strength was illustrated in that study. Based on the scratch test results it was observed that the adherence of the metallizing layer was increasedwiththe increase of the metallization temperature from 1250 ^{o}C to 1400 ^{o}C when time was made constant[4].Figures 3(a-c) represents the cross-sectional SEM images of the Mo-Mn metallized 99.99 wt.%, 96 wt.% and 92 wt.% alumina ceramics, respectively.

Table 1— Properties of alumina ceramics of different purity.

Properties 92 wt.% alumina [4] 96 wt.% alumina [5] 99.99 wt. % alumina.			
Apparent density [g/cm^3]	3.65	3.75	3.75-3.95
Apparent porosity [%]	0	0	0
Water absorption [%]	0	0	0
Microhardness [GPa]	13-14	14-15	15-20
Compressive strength [MPa]	2000	2500	4000
Flexural strength [MPa]	235	260	210-500
Coefficient of thermal expansion [25°C – 1000°C]	8.2×10^{-6}	9×10^{-6}	8.1×10^{-6}
Thermal conductivity at RT [W/m/K]	16.75	-	30-40
Dielectric constant at 1 GHz at RT	6.14	7.32	9.6

SEM observations revealed that the reaction layer thickness increased with increasing the impurity addition in alumina ceramics with respect to the total length of metallizing layer (Fig. 3). As the reaction layer thickness enhanced with increasing impurity in alumina ceramics the thickness of molybdenum containing metallic layer decreased for higher impurity alumina ceramics. It means that the reactivity increases with increasing the rajmahal china clay, CaF_2 and MgF_2 content. During metallization mangano-alumino silicate-based glassy phase was formedat the metallizing layer-substrate interface, which was migrated into the porous metallizing layer by capillary action resulting in bonding between the metallizing layer and the substrate. The formation of the glassy phase was increased with increasing the impurity in the alumina ceramics. Consequently, the reaction layer thickness at the metallizing layer-substrate interface was enhanced with increasing the impurity content in the alumina ceramics[17].

The point and line EDX was performed at the cross-section of metallized 92 wt. % alumina ceramics (Fig. 4). The interfacial region of metallizing layer and reaction layer (spot 3) was consisted of Al, O, Mo, Si, Ca, Mg and Mn elements whereas Mn dominated in spot 2 as indicated by higher percentage of Mn (Fig. 4). EDX analysis showed that complex glassy phase was formed at the substrate-reaction layer interface, which is the main cause of adherence of the substrate with the metallizing layer (Fig. 4). XRD analysis was carried out at the top surface of the reaction layer (Fig. 5). It was noted that the reaction layer was composed of α-alumina, calcium aluminum silicate and amorphous glassy phase. A big hump was present between 10° to 25° of the XRD graph that indicated the presence of amorphous glassy phase. XRD of the reaction layer confirmed the presence of glassy phase (Fig. 5). EDX analysis showed that the reaction region was consisted of Al, Ca, Mn, Si and O

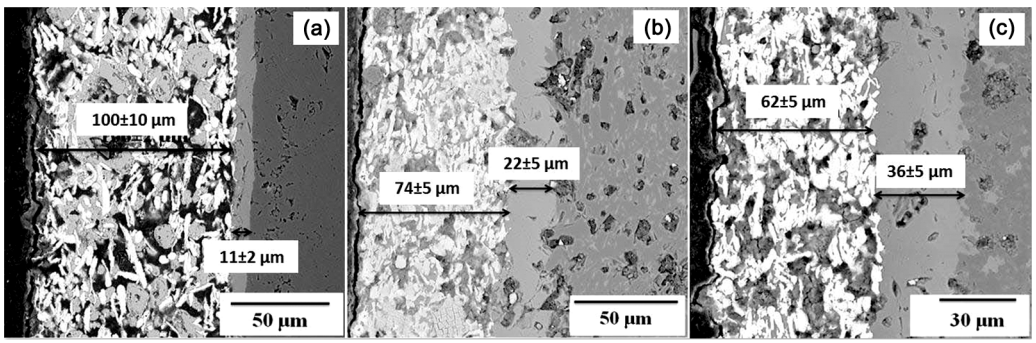

Fig. 3 — Cross-sectional SEM images of Mo-Mn metallized (a) 99.9 wt.%, (b) 96 wt.% and (c) 92 wt.% alumina ceramics.

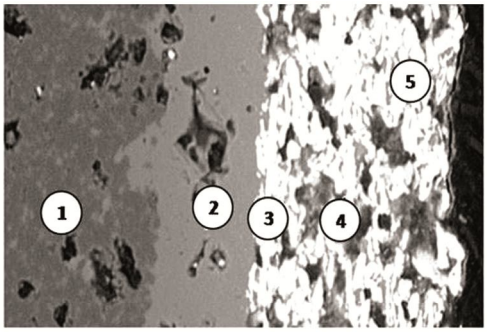

Position	Element name						
	O	Al	Si	Mo	Mn	Mg	Ca
1	53.1	41	2	1.4	1	0.9	0.6
2	55.5	30.2	0.5	2.8	8.4	2.4	0.2
3	45.7	21.1	2.3	23.8	3.8	2.1	1.2
4	54.1	18.2	4	19.6	2.4	0.8	0.9
5	32.1	6.6	2.2	55.6	2	0.7	0.8

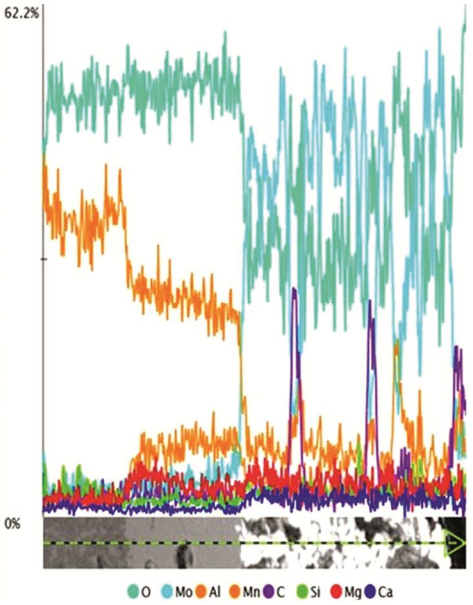

Fig. 4 — Semi-quantitative point EDX analysis and line EDX analysis at different positions of 92 wt.% alumina ceramics.

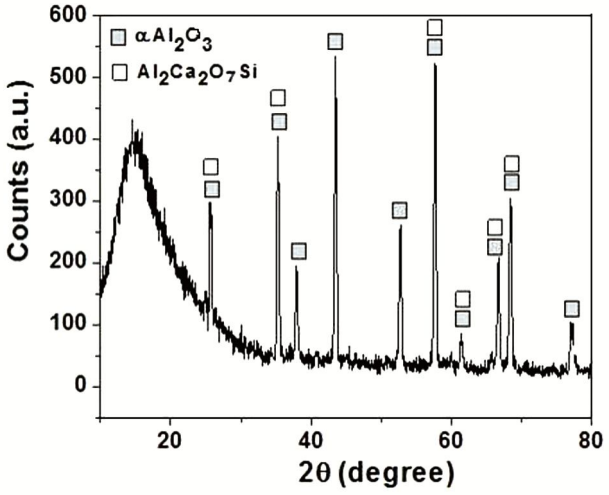

Fig. 5 — XRD analysis at the top surface of the reaction region.

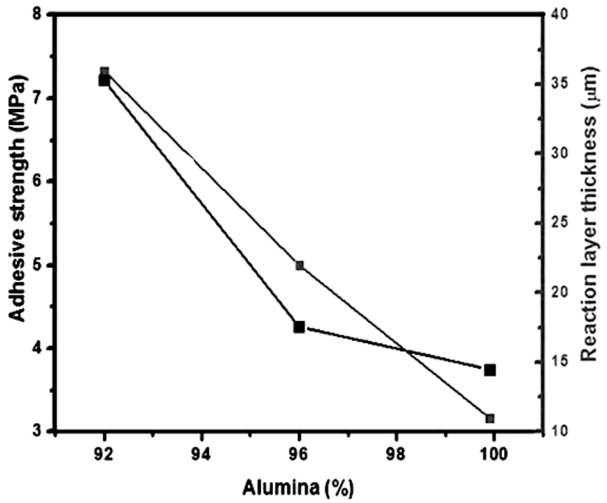

Fig. 6 — Adhesive strength and reaction layer thickness versus alumina content graph.

elements. So, the existence of glassy phase was also supported by the EDX data. EDX analysis supported the XRD results.

Figure 6 represents the adhesive strength and reaction layer thickness versus alumina content graph. The adhesive strength was measured by pull down breaking technique. The adhesive strength and reaction layer thickness decreased with increasing the alumina content. The addition of CaF_2, MgF_2 and SiO_2 as a flux increased the sintering ability of the alumina ceramics. Further, Mn undergoes through the alumina substrate by capillary action and reacts with impurities present in the alumina ceramics resulting in formation of calcium aluminomangano silicate based glass[4,18].Therefore, Mn was detected to be present at the interface of reaction layer and alumina substrate. On the contrary, Mo was present on the top surface of the reaction layer. Addition of higher amount of the flux increased the reaction layer thickness and thereby, increasing the adhesion strength[18-20].Similarly, Zheng*et al.*[21] studied that adhesion strength increased as a function of glass film thickness.

Figures 7 (a and b) shows the SEM image and point EDX at the spots 1 and 2 of Ni coating onto the Mo-Mn metallized alumina ceramics. Ni element was dominated for both the regions (spot 1 and 2). Mo, O, Al, Mn and Si elements were also detected at the top

surface due to diffusion of these elements towards the surface. XRD analysis of the top surface of Ni coating is shown in Fig. 7c. MoNi and Ni phases were identified on the top surface. During formation of nickel coating in hydrogen atmosphere oxygen from NiO reacted with H_2 and formed Ni. Further, Ni reacted with the Mo that was on the upper surface of the metallizing layer and formed MoNi phase. This may be ascribed to the presence of MoNi phase on the surface of nickel coating.

Figures 8 (a and b) represents the SEM images of the cross-section of the conventionally brazed Mo-Mn and Ni coated alumina ceramics using Ag-Cu filler alloy. Figure 8b shows magnified view of the reaction region between the braze and the metallized layer. The whitish and grayish phases were found at the braze region (Figure 8a). Points 1 and 10 showed the presence of Al and O elements as major elements while Mn was present in higher amounts in point 2 and point 9. This was due to the fact that point 2 and point 9 represented the interface of alumina and Mo-Mn metallizing layer. Point 3 showed the presence of Mo in considerable concentration and thereby, indicating that the region was the metallizing layer consisting of mainly molybdenum. In the grayish phase Ag was present in very high percentages as can be seen in points 5 and 6. On the other hand, Cu was identified as whitish phase in points 4, 7 and 8. High amount of Ni was identified in the region marked as points 4 and 8. Nickel was diffused to the braze region during brazing. Thus, Ni was also detected in high concentration in point 7.

The brazed alumina joints could withstand up to $1x10^{-9}$ Torr pressure, which was indicated by helium leak test. Brazing strength was measured for 92 wt. % alumina ceramic joints. Figure 9 shows the maximum brazing strength and maximum applied force graph of the alumina-alumina brazed joint as a function of

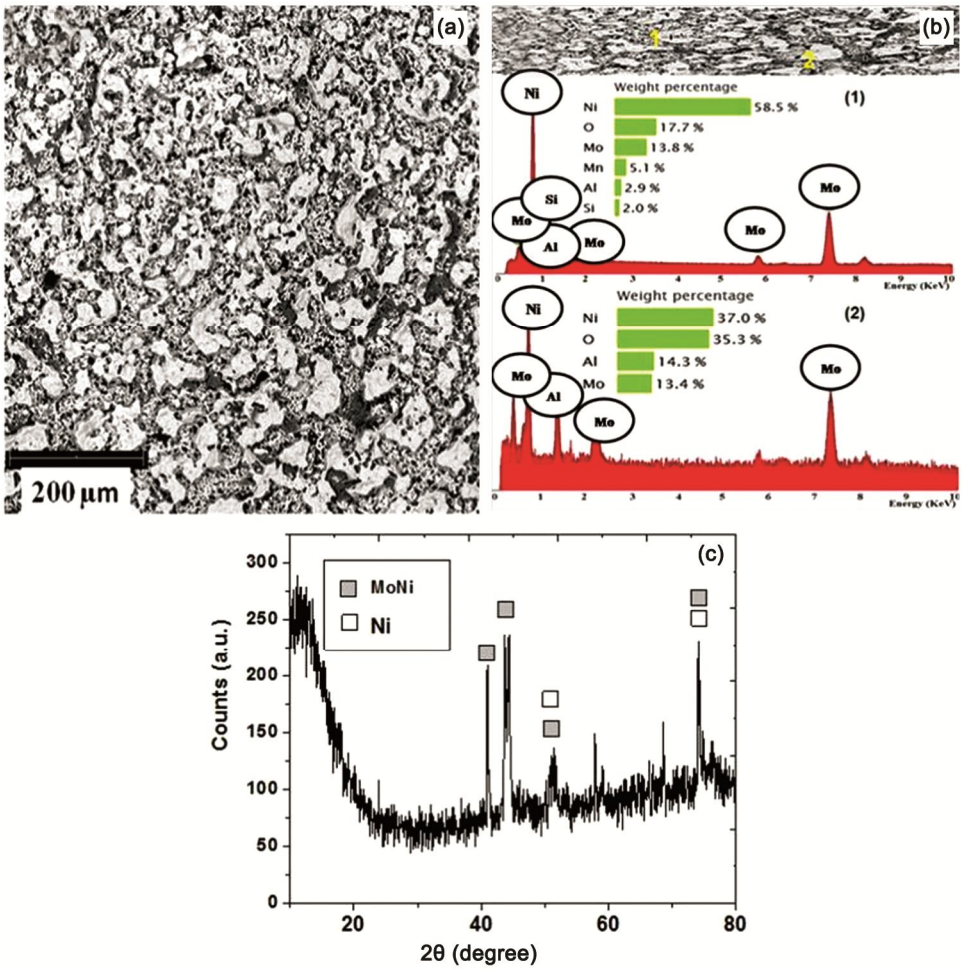

Fig. 7 — (a) SEM image of Ni coated surface after Mo-Mn metallization; (b) semi-quantitative EDX analysis and (c) XRD graph of the nickel coating.

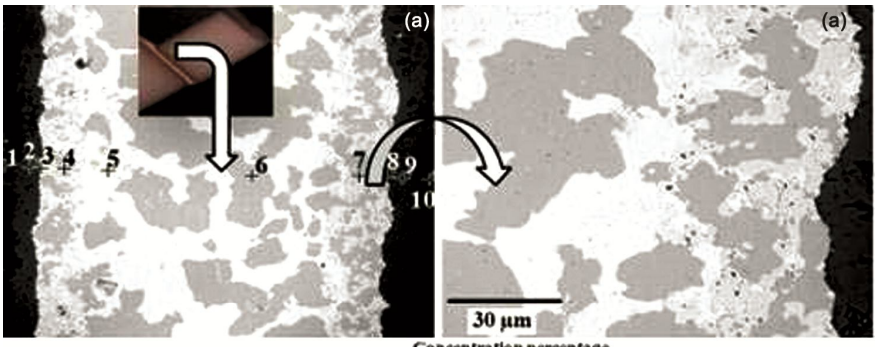

Concentration percentage

Atomic number	Element symbol	Point 1	Point 2	Point 3	Point 4	Point 5	Point 6	Point 7	Point 8	Point 9	Point 10
8	O	49.9	50.2	27	19.9	22.1	18.5	16.5	21	52.1	49.3
13	Al	42.2	32.2	10.8	17.3	10.9	11.1	16.6	20.7	31.7	43.4
47	Ag	2.2	3.6	12.7	9.1	54.9	52.6	6.8	5.8	2.1	1.9
29	Cu	1.7	2.2	3.1	37.4	6.5	12.6	43.5	40	2.5	1.8
42	Mo	1.4	2.5	44.4	11.5	2.3	1.2	5.5	5	2	1.4
12	Mg	1	2.7	0.1	0.9	1.1	1.7	1.2	0.9	2.2	0.9
14	Si	1	0.6	0.5	0.8	0.6	0.8	0.8	0.7	0.5	0.6
25	Mn	0.4	5.7	0.8	0.2	0.6	0	0.4	1.5	6.5	0.4
28	Ni	0.3	0.2	0.6	2.9	1	1.5	8.7	4.6	0.4	0.3

Fig. 8 — (a) and (b) SEM images with (c) point EDX at different positions along the cross-section of brazed joint.

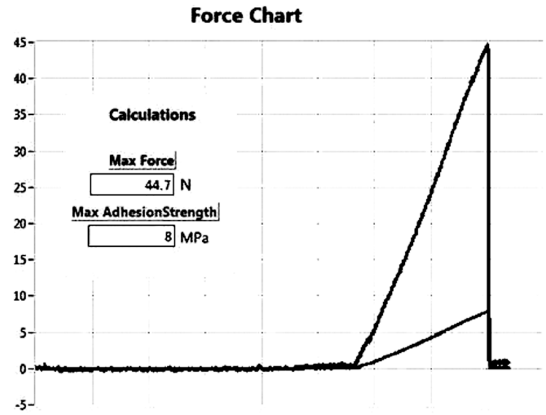

Fig. 9 — Brazing strength and maximum applied force for 92 wt.% alumina brazed joint as a function of time.

time. The joint strength was found to be 8 MPa with the maximum applied force of 44.7 N, which was much lower than the actual value. The alumina brazed joint was found to be quite sound and defect free. No crack was found to be present at the joint interfacial regions. The joint strength was much better than the brazing strength measured by the Romulus universal tester. This is due to the fact that failure of the joint occurred in the alumina portion instead of the joint region.

4 Conclusions

The present study showed that the properties of alumina ceramics are greatly influenced by its impurity content. The properties such as hardness, compressive strength, flexural strength and thermal conductivity degraded with increasing the addition of impurity in the alumina ceramics. Further, it was noted that the thickness of the reaction layer formed at the metallizing layer-substrate interface increased with increasing impurity addition, which directly enhanced the adhesive strength of the metallized layer applied onto the alumina ceramics.Thus, high brazing strength of the alumina ceramic joint was achieved by forming well-adhered metallized layer on the alumina ceramics.

Acknowledgement

The authors acknowledge the financial support of Council of Scientific and Industrial Research (CSIR), India through network project (MTDDC-PSC0101).

References

1 Twentyman ME, *J Mater Sci*, *10 (*1975) *765*.
2 Lamba O S, Nangru S C, Joshi L M, Sharma A, Singh V V P & Gupta N C, *Ind J Eng Mater Sci*, 7 (2000) 443.
3 LiJ & Xiao P, *J MaterSci*, 36 (2001)1383.
4 Ghosh S, Sengupta A, Pal K S, Dandapat N, Chakraborty R, Datta S & Basu D, *Metal Mater Trans A*, 43 (2012) 912.
5 Ghosh S, Pal K S, Dandapat N, Datta S & Basu D, *Metal Mater Int*, 18 (2012) 625.
6 Ghosh S, Chakraborty R, Dandapat N, Pal K S, Datta S & Basu D, *Ceram Int*, 38 (2012) 663.
7 Dandapat N, Ghosh S, Pal K S, Datta S & Guha B K, *Trans Nonferrous Met Soc China*, 24 (2014) 1666.
8 Dandapat N, Ghosh S, Guha B K, Datta S & Balla V K, *Metal Mater Trans B*, 47B (2016) 1.

9 Prodanović V, Chan H W, Graaf H V D & Sarro P M, *Nanotechnol*, 29 (2018)155703.
10 Samandi M, Gudze M & Evans P, *NuclInstrum Methods Phys Res B*, 127/128 (1997) 669.
11 Heo H, Kim G, Park Y-C, Jung K & Kang C-Y, *Metals*, 8 (2018) 752.
12 Milak P C, Minatto F D, Noni A D Jr, Montedo O R K, *Cerâmica*, 61 (2015) 88.
13 Pal KS, Ghosh S, Dandapat N, Datta S, Basu D & Raju R S, *Mater Sci Eng B*,177 (2012) 228.
14 Jana D C, Barick P & Saha B P, *J Mater Eng Perform*, 27 (2018) 2960.
15 Zaidan S A, Hamood A F, Ibrahim S N, *Eng Tech J*, 34 (2016) 610.
16 Louha S P, Leub I C & Hon M H, *DiamRelat Mater*, 14 (2005)1000.
17 Klomp J T & Botden T P J,*Ceram Bull*, 49 (1970) 204.
18 Cho B R, Lee J J & Kang S K, *J Ceram Proc Res*, 10 (2009)121.
19 Liu G W, Qiao G J, Wang H J & Jin Z H, *Key Eng Mater*, 353 (2007) 2049.
20 Liu G W, Qiao G J, Wang H J, Wang J P & Lu T J, *J Mater Eng Perform*, 20 (2011) 1563.
21 Zheng Z, Zhang Y, Yi F, Chen C & Song X, *Ceram Int*, 40 (2014) 12709.